Applied Catalysis B: Environmental 96 (2010) 176–184

Contents lists available at ScienceDirect

Applied Catalysis B: Environmental

journal homepage: www.elsevier.com/locate/apcatb

Uniform dispersion of Au nanoparticles on TiO_2 film via electrostatic self-assembly for photocatalytic degradation of bisphenol A

Pingfeng Fu, Pengyi Zhang*

State Key Joint Laboratory of Environment Simulation and Pollution Control, Department of Environmental Science and Engineering, Tsinghua University, Beijing 100084, China

ARTICLE INFO

Article history:
Received 20 November 2009
Received in revised form 6 February 2010
Accepted 9 February 2010
Available online 16 February 2010

Keywords:
Au–TiO_2 film
Photocatalysis
Nanoparticles
Electrostatic self-assembly
Uniform dispersion
Bisphenol A
Water purification

ABSTRACT

A simple electrostatic self-assembly method was developed to uniformly disperse ultra-fine Au nanoparticles (NPs) on TiO_2 film to improve the photocatalytic activity. Without any modification of TiO_2 surface with functional groups, negatively charged Au NPs could be spontaneously adsorbed on TiO_2 films with electrostatic attraction when the pH of Au colloids was lower than or close to the isoelectric point of TiO_2. Ultra high-resolution FESEM observation showed that Au NPs with diameter of 3–5 nm were physically separated and uniformly dispersed on TiO_2 film. The pH of Au colloids remarkably influenced the Au loading that was decreased at high pH. The average size of deposited Au NPs increased from 3.1 ± 1.3 nm at $-5\,^{\circ}C$ to 10.5 ± 3.1 nm at $40\,^{\circ}C$, indicating that growth of Au NPs was retarded at low temperature. The dispersed Au NPs on TiO_2 film enhanced the photocurrent generation with ~five folds and increased the photovoltage of ~115 mV, revealing that the recombination of electron–hole pairs was significantly reduced. The photocatalytic activity of the Au–TiO_2 nanocomposite film was improved with ~2.5 folds for degradation of bisphenol A, and no deactivation was observed during 10 cyclic tests. The key characteristics of deposited Au NPs, such as ultra-fine size, uniform dispersion, physical separation and high loading, were responsible for improved photocatalytic activity of the Au–TiO_2 film.

1. Introduction

Highly dispersed Au nanoparticles on TiO_2 surface exhibits extraordinary high activity for photocatalytic degradation of undesirable chemical contaminants [1–3]. It has been the focal point of numerous investigations particularly because of the reduction of hole–electron recombination in Au–TiO_2 composites [4–8]. In earlier studies, Au–TiO_2 composite powders were widely investigated [3,9–12]. However, one major drawback, i.e. large cost of separating Au–TiO_2 powder from water after treatment, hinders the practical application. To overcome this obstacle, many investigations are oriented towards immobilization of Au–TiO_2 composites on various supports [13–19].

Up to now, these Au–TiO_2 nanocomposite films have been prepared by both physical and chemical routes, including the RF-sputtering approach [13–15], sol–gel dip coating [16], deposition–precipitation [17,18] and photo-reduction method [19]. To prepare Au–TiO_2 porous films, typically precursor ions like $[AuCl_4]^-$ are first transferred into the pores in advance through adsorption, ion-exchange, or ultra-sonication, then Au precursors are in situ reduced with electrochemical deposition [20], UV irradiation [21] or other chemical methods [22–24]. Then, the reduced Au nanoparticles (NPs) are incorporated into pore channels or matrix of TiO_2 films. However, using these methods, it is difficult to control the morphology, size and distribution of deposited Au NPs due to the influence of oxide supports [25]. Because the photocatalytic activity of Au–TiO_2 composites highly depends on the shape, size, distribution, loading and chemical states of Au NPs [26–28], uniform dispersion of metallic Au NPs with ultra-fine size is vital to improve the photocatalytic activity of Au–TiO_2 composite films.

In recent years, some efforts have been made to uniformly disperse Au NPs on TiO_2 film via assembling pre-synthesized colloidal Au NPs onto the surface of TiO_2, thus the influence of oxide supports in determining the size and dispersion of Au NPs is minimized [29,30]. Additionally, it is much easier to control the size and monodispersity of Au NPs in colloidal solutions than in situ reduction on TiO_2 film [31]. Using the electrophoretic deposition, Patel et al. [25] successfully incorporated 3.1 nm Au NPs inside the mesochannels of TiO_2 film. However, severe agglomerated Au NPs with 20–30 nm diameter appeared on TiO_2 films reported by Kamat and co-workers [4,24]. To electrophoretically deposit Au NPs on TiO_2 films, the substrate must be electrically conductive and Au NPs need to be dispersed in organic medium. With a simple adsorption method, Kamat and co-workers transferred colloidal Au NPs onto the TiO_2 film, but significant agglomera-

* Corresponding author. Tel.: +86 10 62796840x601; fax: +86 10 62796840x602.
E-mail address: zpy@mail.tsinghua.edu.cn (P. Zhang).

0926-3373/$ – see front matter © 2009 Elsevier B.V. All rights reserved.
doi:10.1016/j.apcatb.2010.02.017

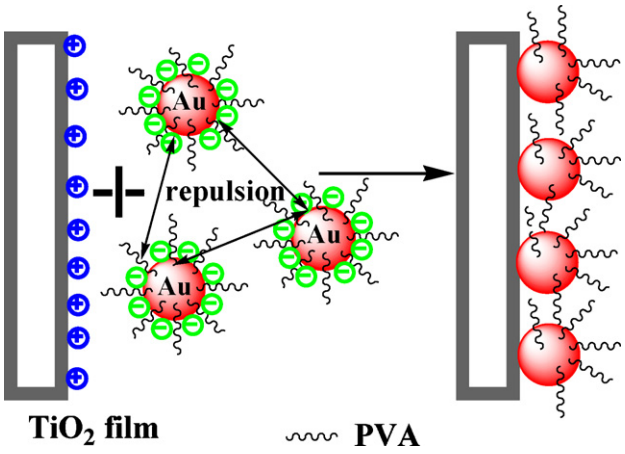

Fig. 1. Illustrative diagram of depositing negatively charged Au nanoparticles on TiO_2 film via electrostatic self-assembly.

tion and growth of Au NPs also occurred [5]. In order to attach colloidal Au NPs on the TiO_2 via self-assembly, the TiO_2 surface is usually modified with functional groups (e.g., SH group) having great affinity to Au NPs [10,32,33]. Although heating treatment can be used to remove these capping agents, the residual sulfur may poison active sites of both Au NPs and TiO_2 support [33,34]. In a word, efficient transfer of pre-synthesized Au NPs from colloidal solutions onto TiO_2 film still remains a great challenge up to now [29–31,33,35].

In this paper, an alternative simple approach is presented that is based on electrostatic self-assembly of colloidal Au nanoparticles (NPs) on prefabricated TiO_2 film (Fig. 1). This strategy provides a completely solution-based method for uniformly dispersion of Au NPs on TiO_2 film. There are several reasons for us to propose this strategy: (1) the ultra-fine size, well-distribution and tailored loading of Au NPs can be obtained by easily controlling over the pH and temperature of Au colloids and assembly time. (2) Physical separation of individual Au NPs can maximize the transfer efficiency of photo-generated electrons from TiO_2 to Au NPs. (3) Due to the ease of fabrication, this route is low cost and scalable to fabricate various Au–TiO_2 nanocomposite films with no restrictions on the size, shape or composition of the supports.

Bisphenol A (BPA) is widely used as a major component for manufacturing polycarbonate resins, epoxy and polyester-styrene resins [36,37]. And it is a well-known endocrine disrupting chemical (EDC) due to its estrogenic activity [38]. Thus, the inevitable discharge of BPA from plastic products has caused severe water pollution. Effective treatment of BPA has been required as part of water remediation efforts. In this work, BPA is adopted as a model compound to evaluate the photocatalytic activity of the prepared Au–TiO_2 film.

2. Experimental

2.1. Chemicals

All chemicals were used as received without further purification. Polyvinyl alcohol (PVA, 99.0%, average molecule weight 1750), sodium borohydride, tetrabutylorthotitanate, acetyl acetone, *n*-propanol, hydrocholoric acid and sodium hydroxide were purchased from Beijing Chemical Reagent Company. Hydrogen tetrachloroaurate trihydrate ($HAuCl_4{\cdot}3H_2O$) and bisphenol A were from Sigma–Aldrich. Ultra-purity water from Thermo Barnstead Nanopure Diamond UV^{TM} was used in all experiments.

2.2. Synthesis of Au–TiO_2 nanocomposite film

TiO_2 film was prepared with a sol–gel dip-coating method similar to our previous study [39]. Tetrabutylorthotitanate, acetyl acetone, water and *n*-propanol were mixed with a volumetric ratio of 1:0.3:0.4:7. The titanium sheet, pretreated with 10 wt% hot oxalic acid solution, was dipped into the above sol and withdrawn at a speed of 1 mm s^{-1}. The dried gel film was annealed in air at 500 °C for 1 h at a heating rate of 2 °C min^{-1}. After four cycles of the dip-coating process, the film with optimized TiO_2 loading was coated on the Ti substrate.

The typical procedure for depositing Au nanoparticles (NPs) on the TiO_2 film is given as follows. 354 mg PVA was dissolved into $HAuCl_4$ aqueous solution (0.3 mM, 200 mL). Then, the PVA/$HAuCl_4$ solution was kept at low temperature in a water bath, into which a fresh $NaBH_4$ solution (0.07 M, 10 mL) was rapidly added with simultaneous ultra-sonication and vigorous stirring for 1 min. The color of the mixture immediately turned from pale yellow to dark brown, indicating the formation of Au NPs. A piece of prefabricated TiO_2/Ti sheet, 150 mm × 120 mm, was rolled up and completely immersed into the freshly prepared Au colloids. By adjusting the pH of Au colloids, the Au NPs were adsorbed on the TiO_2/Ti sheet via electrostatic self-assembly at low temperature in a static manner. After assembly of 5–90 min, the TiO_2/Ti sheet was withdrawn, washed with boiling water for 3 times, and then annealed in air at 300 °C for 1.5 h to remove the capped PVA. Thus, the Au–TiO_2 nanocomposite films with various Au loadings were prepared.

2.3. Characterization

The morphology of Au–TiO_2 film was observed using an ultra high-resolution field-emission scanning electron microscope (FESEM, S-5500, Hitachi, second electron resolution: 0.4 nm/30 kV) performed at an accelerating voltage of 5.0 kV. X-ray from the SEM microscope probe was used to determine the deposited Au amount. High-resolution transmission electron microscopy (HRTEM) images were recorded using a JEM 2010 microscope with an electron diffractometer. The zeta potentials of Au colloids and TiO_2 films were measured as a function of pH using a zeta potential analyzer (ZetaPALS, 32BIT, Brookhaven). The UV–Vis absorption spectra of Au colloids were recorded using a UV-Vis Recording Spectrophotometer (UV-2401PC, Shimadzu). TiO_2 and Au–TiO_2 powders for recording TEM images and zeta potentials were scratched from the Ti substrate. X-ray diffraction (XRD) analysis of the TiO_2 and Au–TiO_2 films was carried out with a Rigaku D/max-RB using Cu Kα radiation (λ = 0.15418 nm), operated at 40 kV and 100 mA.

Chemical states of surface elements of the films were investigated by X-ray photoelectron spectroscopy (XPS, PHI-5300, ESCA) at a pass energy of 50 eV, using Al Kα as an exciting X-ray source. The spectra were calibrated with respect to the C1s line of adventitious carbon at 284.8 eV. Elemental analysis of Au–TiO_2/Ti was conducted with an inductively coupled plasma-atomic emission spectrometry (ICP-AES, IRIS Intrepid II XSP). The Au–TiO_2/Ti sheets with a size of 150 mm × 120 mm were first dissolved in aqua regia for 24 h. The solution containing Au ions was then analyzed to determine the Au loading.

2.4. Photoelectrochemical measurements

The photoelectrochemical measurements were performed by using a CHI 660B electrochemical workstation in a classical three-electrode electrochemical cell with reference (saturated calomel electrode, SCE)) and counter (platinum foil) electrodes. The TiO_2/Ti or Au–TiO_2/Ti sheet, with area of 2 cm^2, acted as the working electrode. The electrolyte was N_2-saturated 0.05 M Na_2SO_4 solution.

The UV illumination was provided with a 3 W low-pressure mercury lamp (λ_{max} = 254 nm) fixed in the center of cell.

2.5. Photocatalytic degradation of bisphenol A

The photocatalytic activity of the Au–TiO_2/Ti or TiO_2/Ti photocatalysts was evaluated by degrading bisphenol A (BPA). The reactor consisted of a 120 mL cylindrical vessel, into which the TiO_2/Ti or Au–TiO_2/Ti sheet with a size of 150 mm × 120 mm was inserted. A 10 W low-pressure mercury lamp (λ_{max} = 254 nm) was perpendicularly placed in the center of the reactor. The aqueous solution of BPA (30 mg L^{-1}, 600 mL) was circulated through the reactor by a peristaltic pump. An oxygen flow was supplied into the reactor with a flow rate of 30 mL min^{-1}. After the adsorption equilibrium reached, the UV lamp was turned on to carry out the photocatalytic reaction. The 0.5 mL solution was sampled at certain time intervals, and the concentration of BPA was determined using a high-performance liquid chromatography (HPLC, Shimadzu, LC-10AD) with a UV detector (SPD-10AV) at 276 nm and a Kromasil C18 column (250 mm × 4.6 mm) for separation. The mobile phase was a mixture of methanol and water (70:30, v/v) at a flow rate of 0.8 mL min^{-1}. The TOC of the sampled solution was determined with a Total Organic Carbon Analyzer (Shimadzu, TOC-V_{wp}).

3. Results and discussion

3.1. Electrostatic self-assembly strategy

The general self-assembly strategy for immobilizing colloidal Au nanoparticles (NPs) on metal oxides involves modification of the supports with organic agents, which have bi-functional groups with high affinity for Au (i.e., CN, SH, NH_2) [10,40,41]. To avoid the shielding of active sites of TiO_2 and the poisoning of catalytic activity of Au–TiO_2 by functional organics, the electrostatic self-assembly is developed to directly adsorb charged Au NPs on unmodified TiO_2 film with no restriction on size and shape (Fig. 1). By adjusting the pH of Au colloids close to or lower than the isoelectric point of TiO_2, negatively charged Au NPs protected by PVA are spontaneously adsorbed on positively charged sites of TiO_2 film. This self-assembly process is thermodynamically driven and depends on the electrostatic attraction between TiO_2 film and Au NPs. After adsorbed, the Au NPs have little possibility to diffuse back into the bulk solution due to the strong electrostatic attraction to the TiO_2. Both the electrostatic repulsion among charged Au NPs and steric hindrance effect of capped PVA reduce the surface mobility of the deposited Au NPs and prevent the spontaneous coalescence of Au particles on the TiO_2 surface.

The TiO_2 film, with the anatase fraction of 62.5% and rutile of 37.5% (XRD result, not shown), was used as substrate to deposit Au NPs. Fig. 2 shows the overall view of the Au–TiO_2 nanocomposite film prepared with above-mentioned electrostatic self-assembly approach. As shown in Fig. 2a, the Au NPs, after annealed in air at 300 °C for 1.5 h, are highly dispersed on the TiO_2 film with a size of 3–5 nm. The small Au particle size shows the good thermal stability of loaded Au NPs in the calcination [22]. This extremely uniform dispersion of Au NPs can be found across a large area of TiO_2 film. The loaded Au NPs are physically separated on TiO_2 film with an interparticle spacing of 5–20 nm. The high-resolution FESEM image indicates that nearly 2–3 Au NPs have coated on each TiO_2 particle. To exactly reveal the microstructure of the Au–TiO_2 composite, the powder sample scraped from the Ti support was subjected to TEM test. As shown in Fig. 2b, the loaded Au NPs, with an approximate spherical shape, have the diameter of 3–5 nm, which is well agreed with the FESEM observation. The Au NPs are highly crys-

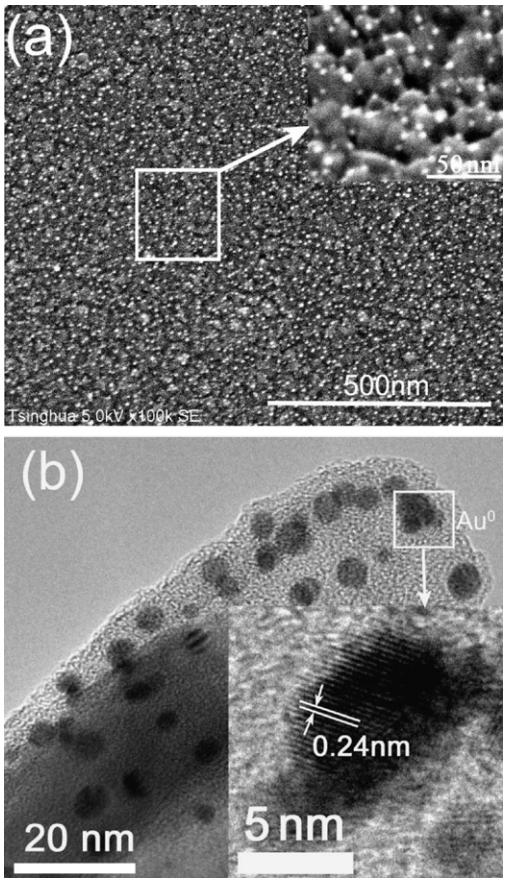

Fig. 2. Overall view of Au–TiO_2 nanocomposite film: (a) FESEM image (the white dots are Au nanoparticles), and (b) TEM image (the inset is the HRTEM image of supported Au nanoparticles).

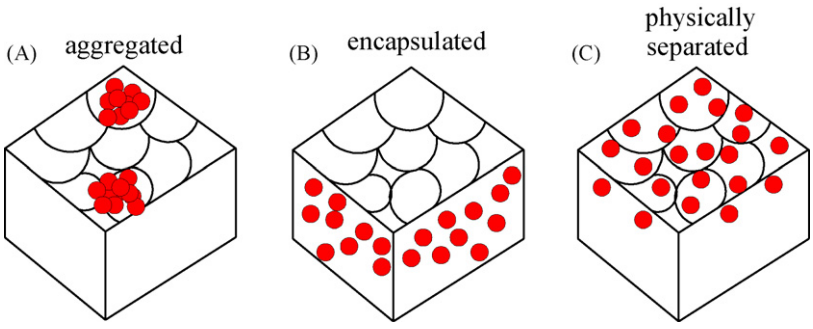

Fig. 3. Three morphologies of Au nanoparticles (red circle) deposited on TiO_2 film. (For interpretation of the references to colour in this figure legend, the reader is referred to the web version of the article.)

Table 1
Effect of the pH on the zeta potential (ζ) of Au colloids and TiO_2, Au weight percentage, loading, average size and surface density of deposited Au nanoparticles on TiO_2 films.

pH	Zeta potential (mV)		Au weight percentage (wt%)[a]	Au loading ($\mu g\,cm^{-2}$)[b]	Average size (nm)[c]	Surface density ($NPs\,cm^{-2}$)[d]
	Au colloids	TiO_2				
2.2	−0.45	13.94	1.71	3.35	5.8 ± 1.4	2.51×10^{11}
3.9	−0.98	3.75	1.48	3.05	4.3 ± 1.2	5.07×10^{11}
5.8	−1.40	−6.52	1.32	2.83	4.1 ± 0.9	4.94×10^{11}
8.4	−2.50	−19.15	0.82	1.73	3.8 ± 1.1	3.93×10^{10}
9.9	−3.10	−20.88	0.77	1.55	3.9 ± 0.8	1.72×10^{10}

[a] The Au weight percentage was measured by EDX on an area of 150 μm × 150 μm.
[b] The Au loading is obtained by ICP-AES analysis.
[c] The average diameter of Au nanoparticles and the standard deviation were calculated by measuring the core diameters of more than 240 particles.
[d] The surface density (particle number per unit area) was obtained by manually counting the number of Au NPs in the FESEM images taken at different points of the Au–TiO_2 film surface. The error percent in the analysis of the surface density is within 10%.

tallized as evidenced from the well resolved Au(1 1 1) (0.24 nm) crystalline lattices [42]. But the diffraction peaks of metallic Au NPs does not appear when the Au–TiO_2 film was subjected to XRD test (not shown). This may be due to the low Au loading on TiO_2 film. As illustrated in Fig. 2, no obvious aggregation of Au NPs is observed even though the Au NPs on TiO_2 film tend to wet the TiO_2 surface during calcination. This can be attributed to physical separation and strong surface confinement to TiO_2 surface of individual Au NPs. In our attempt to control the size, distribution, monodispersity and loading amount of the adsorbed Au NPs, the pH and temperature of Au colloids were found to be two vital factors as described below.

Fig. 3 depicts three morphologies for Au NPs deposition on TiO_2 films that could result from various synthesis routes. In Fig. 3A, the Au NPs have aggregated to islands on the TiO_2 surface by adsorbing [5] or electrophoretic deposition [4,24] of colloidal Au NPs on TiO_2. In Fig. 3B, most of Au NPs have been encapsulated in the bulk TiO_2 film with the sol–gel dip-coating method [16] or the sono-chemical and photochemical route [21]. Fig. 3C represents the physically separated individual Au NPs on TiO_2 film in this work. There are many advantages to keep the Au NPs physically separated and highly dispersed on the TiO_2 film. First, the transfer efficiency of photo-induced electrons from TiO_2 to Au NPs is increased. The electrons have more chance to be transferred to Au NPs. As exemplified by Bowker et al. [43], the larger the metal–support boundary, the higher the reaction rate. The total length of the boundary between Au NPs and TiO_2 surface become longer while 2–3 Au NPs is physically separated on each TiO_2 particle. Second, the contact area of Au NPs to TiO_2 surface is improved. If the Au NPs are aggregated into island shape (Fig. 3A), most of TiO_2 surface is "nude" without covering Au NPs. Third, the capture of electrons on Au NPs by dissolved oxygen molecules at the solid-liquid interface is enhanced if Au NPs are dispersed on TiO_2 surface other than encapsulated into the bulk TiO_2 film (Fig. 3B).

3.2. Effect of colloidal pH on Au loading

The pH value can remarkably influence the zeta potential (ξ) of both Au colloids and TiO_2 surface [31,44], so it is a vital factor to determine the Au loading in the electrostatic self-assembly route. Fig. 4 shows the FESEM images of dispersion of Au nanoparticles

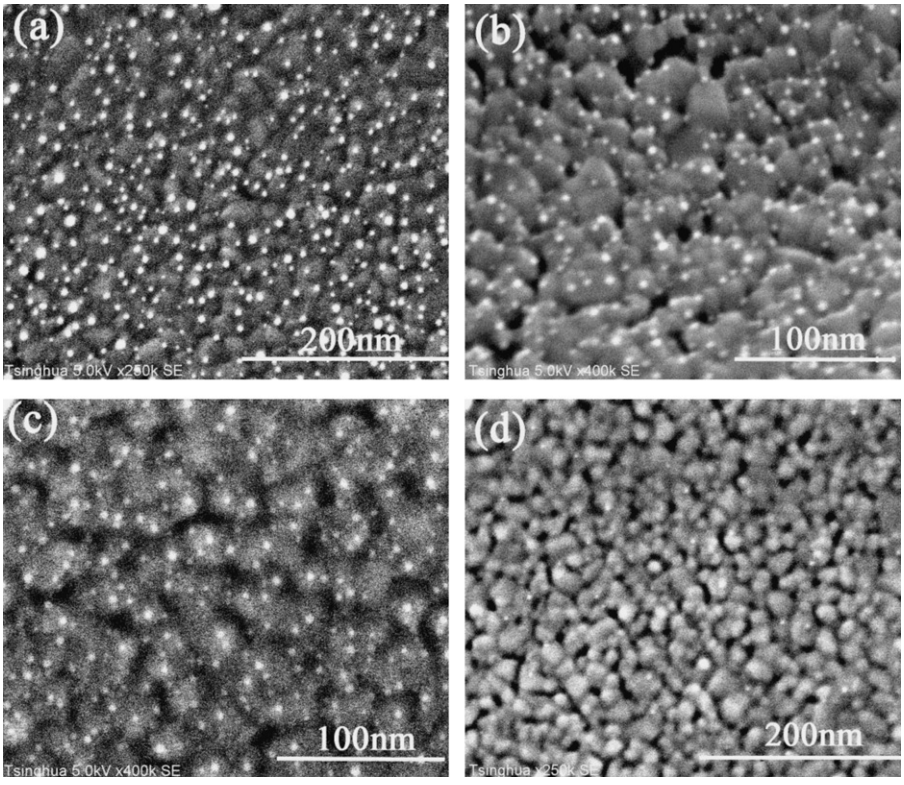

Fig. 4. FESEM images (top down view) of Au nanoparticles deposited on TiO_2 film at pH of 2.2 (a), 3.9 (b), 5.8 (c) and 8.4 (d). The self-assembly processes were conducted at 0 °C for 30 min.

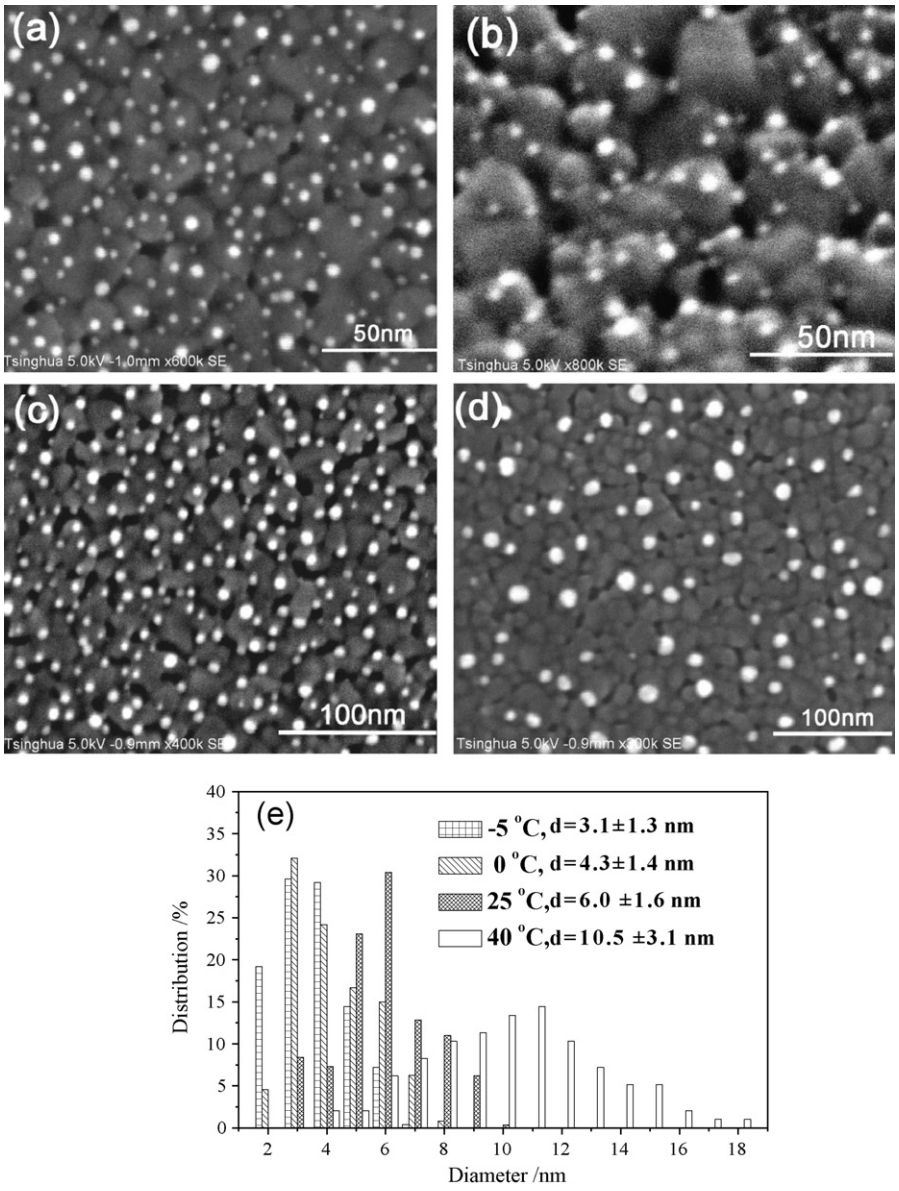

Fig. 5. FESEM images of Au nanoparticles dispersed on TiO_2 films at different temperatures of Au colloids: (a) −5 °C; (b) 0 °C; (c) 25 °C; (d) 40 °C; (e) size distribution histogram of deposited Au nanoparticles. The self-assembly processes were conducted at pH of 3.9 for 30 min.

(NPs) on TiO_2 film at different pH values. The effect of pH on zeta potential of both Au colloids and TiO_2, and several parameters of deposited Au NPs are summarized in Table 1. It is very clear that the weight percentage, Au loading and surface density (particle number per unit area) of the Au NPs become higher at lower pH. In particular, as shown in Fig. 4d, only sparse Au NPs (white dots) are observed at pH 8.4. As listed in Table 1, the ξ of Au colloids is −0.45 to −3.1 mV at pH ranging from 2.2 to 9.9, and the isoelectric point (IEP) of the prepared TiO_2 is ca. 5.5. When the pH is higher than the IEP, the TiO_2 film surface is negatively charged, and thus it is difficult for the same negatively charged Au NPs to be adsorbed onto TiO_2 films due to the electrostatic repulsion. On the contrary, as the pH is lower than or close to the IEP, the Au NPs can be spontaneously adsorbed on TiO_2 surface due to the electrostatic attraction. In this self-assembly route, the coulombic charge of the TiO_2 determines the interaction strength with PVA capped Au NPs [29]. Although the Au–TiO_2 film was washed with hot water for 3 times before calcination, a large amount of Au NPs were surely dispersed on the TiO_2 film as evidently shown in Fig. 4, indicating the strong interaction between the TiO_2 support and charged Au NPs.

As shown in Table 1, the size of deposited Au NPs becomes smaller as the pH increases, indicating the lower possibility of agglomeration. Because the ξ of Au colloids is more negative at high pH, the electrostatic repulsion among them becomes stronger [45]. Thus, the agglomeration of Au NPs is remarkably inhibited at high pH.

The Au loading on TiO_2 film obtained in this work is higher than or close to reported ones by electron beam evaporation [1], photo-reduction [18,19] and sol–gel method [16], but much lower than that deposited by electrophoretic approach [24,25]. The size of deposited Au NPs can be tailored to 4–5 nm, which is much smaller than that prepared by electron beam evaporation [1] and photo-reduction [18,19]. Therefore, the electrostatic self-assembly at low temperature can be used to uniformly deposit Au NPs on the TiO_2 films with the tailored size, distribution and Au loading.

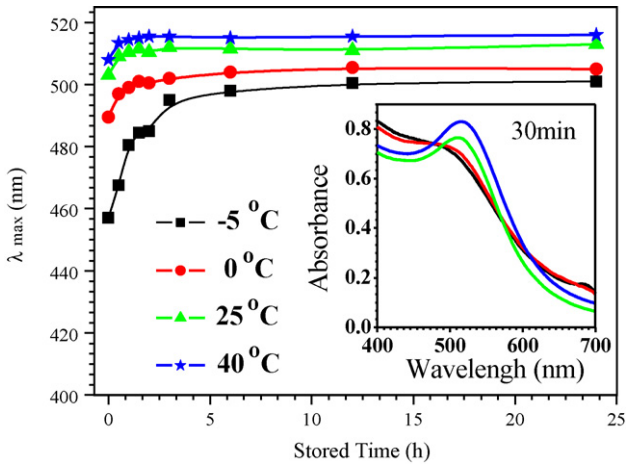

Fig. 6. Wavelength of adsorption maximum (λ_{max}) of Au colloids as a function of time stored at −5, 0, 25 and 40 °C. The inset is the optical absorption spectra of Au colloids stored at different temperatures for 30 min.

3.3. Effect of temperature of the colloids on deposited Au size

In the literature [41,46,47], low temperature was employed to prepare and store seed Au clusters with a diameter of 1–2.5 nm, indicating that the low temperature can inhibit the growth of colloidal Au clusters. But the effect of temperature of the colloids on the growth of Au nanoparticles (NPs) has not yet been well investigated. In this electrostatic self-assembly route, the temperature of Au colloids is found to remarkably influence the average size of deposited Au NPs. The high-resolution FESEM images of Au NPs dispersed on TiO_2 film at different temperatures are shown in Fig. 5. Although Au NPs are well dispersed on TiO_2 film at the temperature ranged at −5–40 °C, the size of deposited Au NPs increases from 3.1 ± 1.3 nm at −5 °C to 10.5 ± 3.1 nm at 40 °C. Especially, a large amount of Au NPs with <3 nm diameter are loaded on TiO_2 surface at low temperature of −5 °C (Fig. 5a) or 0 °C (Fig. 5b). Obviously, the low temperature of Au colloids has significantly inhibited the growth of loaded Au NPs. As mentioned-above, nano-scale surface motion of Au NPs on TiO_2 surface has been prevented due to the strong electrostatic attraction to the TiO_2 support and steric hindrance of capped PVA. Therefore, the possibility of agglomeration of ultra-fine Au NPs to larger ones is very low as soon as the colloidal Au NPs are adsorbed on TiO_2 surface. Herein, the growth of loaded Au NPs dependent on the temperature presumably results from the aggregation and growth of colloidal Au NPs in aqueous solutions at the raised temperature.

To testify the above viewpoint, we performed the UV–Vis spectroscopic measurement of Au colloids to examine the evolution of maximum adsorption peaks (so-called surface plasma bands) as a function of stored time at different temperatures. As shown in Fig. 6, the wavelength of maximum adsorption (λ_{max}) of all of Au colloids increases at the beginning stage, which indicates the growth of ultra-fine Au clusters just after they are reduced by $NaBH_4$. But this kind of Au growth will almost stop when the aging/storing time increases up to 0.5–3.5 h, depending on the temperature. However, the stable λ_{max} of Au colloids increases from 498 nm at −5 °C to 515 nm at 40 °C, indicating that the size of colloidal Au NPs has increased with increase in temperature [47,48]. As shown in the insert of Fig. 6, the surface plasma peak nearly disappears at low temperature of −5 or 0 °C, while the absorption peak is very strong at 25 or 40 °C. The UV–Vis spectra of Au colloids show that the low temperature can surely prevent the growth of colloidal Au NPs. So by keeping the electrostatic self-assembly at low temperature, ultra-fine Au NPs can be uniformly dispersed at the surface of TiO_2 film.

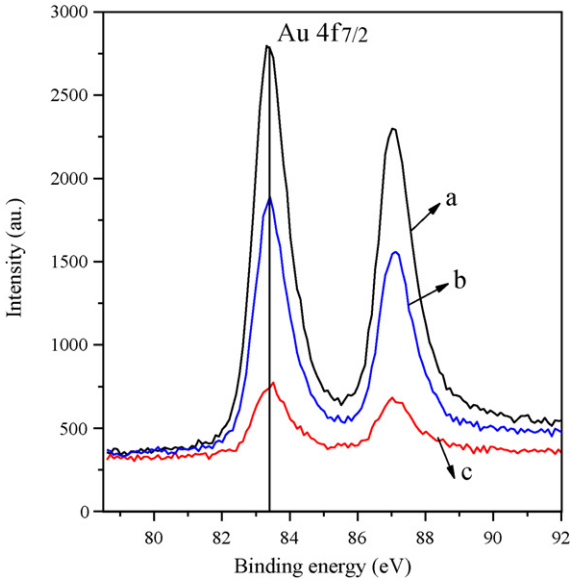

Fig. 7. The Au 4f XPS spectra of the Au–TiO_2 films synthesized at pH 2.2 (a), 5.8 (b) and 8.4 (c). The self-assembly processes were conducted at 0 °C for 30 min.

3.4. Chemical state of deposited Au nanoparticles

To determine the chemical valence state of Au NPs, X-ray photoelectron spectroscopy (XPS) was performed. The Au 4f XPS spectra of Au–TiO_2 films prepared at various pH values were obtained (Fig. 7). The Au $4f_{7/2}$ peaks of three samples are centered at the same binding energy of 83.5 eV, indicating the metallic Au particles. But a shift of ~0.5 eV is observed from the binding energy of bulk metallic gold (84.0 eV) [49]. This shift toward lower value can be ascribed to the small size and negative charging of Au nanoparticles (NPs). It is reasonable that electron transfer is facilitated from TiO_2 support to Au NPs due to large difference in the work function between Au (5.27 eV) [50] and TiO_2 (4.1 eV) [51]. This phenomenon may become more intense for smaller Au NPs due to the decreased coordination number of surface Au atoms [52]. The difference in peak intensity of Au $4f_{7/2}$ peaks reveals that the sample prepared at lower pH has higher Au loading, which is consistent with the measured results by ICP-AES and EDX (Table 1).

3.5. Photoelectrochemical characteristics

The photocurrent time profiles of the Au–TiO_2/Ti and TiO_2/Ti electrodes to UV irradiation are shown in Fig. 8. The photocurrent generation was prompt and the current was stable in the time interval of the pulsed illumination. The observed photocurrent is nearly five-fold higher for the Au–TiO_2/Ti than the TiO_2/Ti electrode. Obviously, the separation of photo-generated holes and electrons has been greatly improved by dispersing Au NPs on TiO_2 surface.

The magnitude of the photovoltage (open-circuit potential, V_{oc}) represents the energy difference between the apparent Fermi level of the TiO_2 film and the reduction potential of the redox couple in the electrolyte [4]. We measured the open-circuit potentials (V_{oc}) of the TiO_2/Ti and Au–TiO_2/Ti electrode at various pH values (Fig. 9). The absolute value of V_{oc} increases with increasing pH as the conduction band shifts to more negative potential [5]. The Au–TiO_2/Ti electrode consistently yields more negative V_{oc} (~115 mV) than the TiO_2/Ti electrode, while it maintains a similar slope of ~44.5 mV pH^{-1} to that of TiO_2/Ti. These observations also confirm that the adsorbed Au NPs improve the accumulation of electrons within the TiO_2 film by facilitating the holes transfer at the electrolyte interface [5]. In the present work, physically isolated

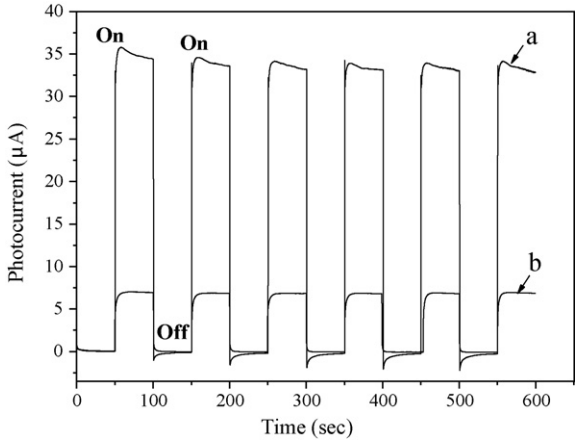

Fig. 8. The photocurrent response of the Au–TiO_2/Ti (a) and TiO_2/Ti (b) electrodes to UV irradiation.

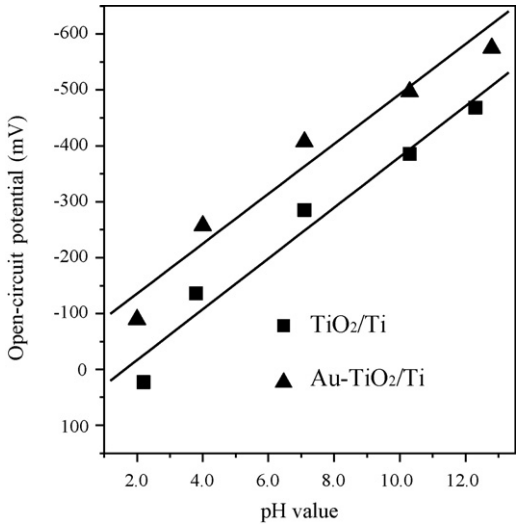

Fig. 9. Dependence of the open-circuit potential (V_{oc}) on the pH value following UV irradiation of the TiO_2/Ti and Au–TiO_2/Ti electrodes.

and highly dispersed Au NPs on TiO_2 films, with 2–3 Au NPs per each TiO_2 particle, have maximized the transfer efficiency of photogenerated electrons from TiO_2 to Au NPs. So the recombination of electron–hole pairs is greatly reduced.

3.6. Photocatalytic activity for degrading bisphenol A

To evaluate the photocatalytic activity of the prepared Au–TiO_2 film, the samples with different Au loadings were synthesized by varying assembly time (5–90 min), which was conducted at 0 °C and pH 3.9. The experimental results of the photocatalytic degradation of bisphenol A (BPA) is shown in Fig. 10 and summarized in Table 2. Less than 7% reduction of BPA is observed by 254 nm

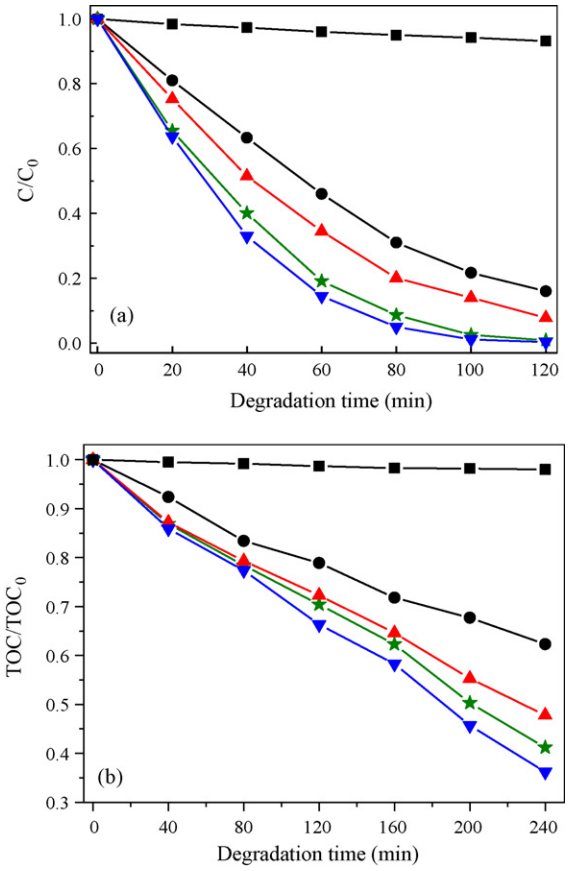

Fig. 10. Time dependent of relative concentration of bisphenol A (a) and relative TOC (b) with 254 nm UV photolysis (■) and using selected Au–TiO_2/Ti catalysts with Au loading of 0 (●), 1.6 (▲), 2.72 (⋆) and 3.04 μg cm^{-2} (▼).

UV direct photolysis. The photocatalytic degradation of BPA obeys the apparent first-order reaction kinetics. As shown in Fig. 10 and Table 2, both the degradation of BPA itself and removal of TOC are enhanced as the Au loading increases. Due to the formation of various intermediates such as 4-vinylphenol, *p*-hydroxyacetophenone and *p*-hydroxybenzaldehyde [36,38], the removal ratio of TOC is far lower than that of BPA. In this study, the pure TiO_2 film decomposes BPA with an apparent first-order rate constant (k') of 0.0171 min^{-1}. At the Au loading of 3.04 μg cm^{-2}, we obtained an enhancement of ~2.5 folds of the k' as compared to pure TiO_2 film. By further increasing the Au loading, the reaction rate decreases due to the inability of the holes to reach the interface as well as an increased light-shielding effect of the gold particles [53]. In the Au–TiO_2 composites, the particle size of Au NPs also has the effect on the photocatalytic activity. The apparent Fermi level of the Au–TiO_2 composite negatively shifts as the size of Au NPs decreases from 8 nm to 3 nm, showing higher charge separation capacity for smaller Au NPs [54]. The higher charge separation efficiency also leads to higher rate of HO• radicals formation and facilitates O_2

Table 2
Effect of the Au loading on the reaction rate constant k', removal ratio of BPA at 120 min and removal ratio of TOC at 240 min.

Au loading (μg cm^{-2})	Reaction rate constant k' (min^{-1})	Removal ratio of BPA at 120 min (%)	Removal ratio of TOC at 240 min (%)
0	0.0171	84.1	37.7
1.6	0.0286	92.2	52.2
2.05	0.0342	94.6	54.3
2.2	0.0372	95.2	56.1
2.72	0.0399	99.1	58.8
3.04	0.0431	99.7	63.8
3.75	0.0398	98.7	56.9

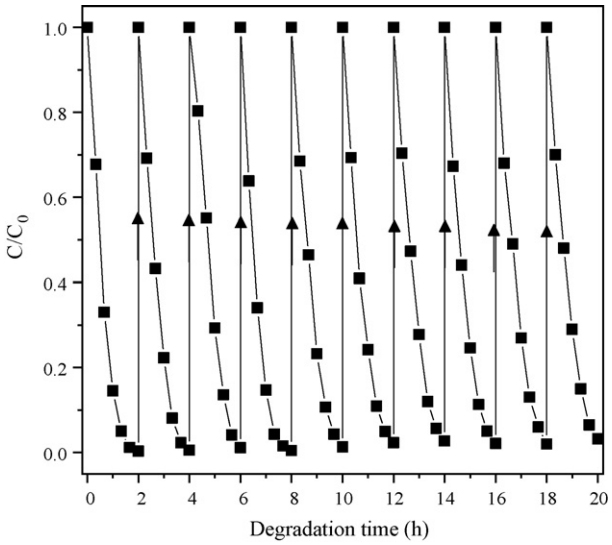

Fig. 11. Photocatalytic performance of the Au–TiO_2 film with the Au loading of 3.04 μg cm^{-2} in the 10 cyclic degradation tests.

reduction, which are the rate-limiting steps for oxidizing adsorbed organic pollutants on TiO_2 surface [55]. In the literature [9,55,56], the Au size smaller than 4 nm exhibits the highest photocatalytic activity of Au–TiO_2 composites. So the mean size of ~4 nm of loaded Au NPs may be an appropriate size to enhance photocatalytic oxidation of BPA in this work.

The result suggests that uniformly dispersed Au NPs play a significant role in facilitating the interfacial charge transfer and inhibiting the recombination of photo-generated hole–electron pairs, as revealed by enhanced photoelectrochemical performances. In this study, the good microstructures of highly dispersed, ultra-fine and well-distributed Au NPs on TiO_2 films may greatly contribute to the increased activity, because the photocatalytic reaction of decomposition of the pollutants mainly occurs on the film surface.

The long-term photocatalytic performance of the Au–TiO_2 film was tested by repeating the photocatalytic degradation of BPA. As shown in Fig. 11, the removal ratio of BPA is kept at nearly 100% in 2 h as the photocatalytic run increases to 10 cycles, indicating that the photocatalytic activity of the Au–TiO_2 film has little change during these 10 runs. Because the photocatalytic activity is highly dependent on the Au loading as shown in Fig. 10, the loss of deposited Au NPs should be little in the 20 hours' test. In the washing process of removing Cl^- anions before calcination, some loosely attached Au NPs have been washed off in the hot water. After the removal of capped PVA by calcination, the adsorbed Au NPs should be tightly bound to the TiO_2 film [29]. The measured Au $4f_{7/2}$ binding energy of the Au–TiO_2 sample after 10 cyclic degradations is 83.45 eV, which is very close to the Au $4f_{7/2}$ binding energy (83.5 eV) of Au NPs before the usage. It implies that small Au NPs have not been oxidized by holes [28].

4. Conclusions

Highly dispersed Au nanoparticles (NPs) on TiO_2 film has been successfully synthesized through a simple electrostatic self-assembly route. The size, distribution and loading amount of deposited Au NPs can be easily tailored by adjusting pH and temperature of Au colloids and assembly time. A low temperature of Au colloidal solution can significantly inhibit the agglomeration and growth of deposited Au NPs. Ultra high-resolution FESEM observation shows that ultra-fine Au NPs with 3–5 nm diameter are uniformly dispersed on TiO_2 film. The physical separation and tight surface confinement to TiO_2 surface of deposited Au NPs has improved the transfer efficiency of photo-generated electrons from TiO_2 to Au particles. The photocatalytic activity of the Au–TiO_2 nanocomposite film is improved by ~2.5 folds as compared to the pure TiO_2 film. This can be attributed to the remarkably reduced recombination of hole–electron pairs, as revealed by the increased photocurrent and photovoltage of Au–TiO_2 film. The immobilized Au–TiO_2 film with large area exhibits high activity and stability in the photodecomposition of bisphenol A, showing good potential for application in wastewater treatment. More importantly, the developed electrostatic self-assembly route is simple, low cost, and scalable to fabricate Au–TiO_2 films with various size, shape and composition of the supports.

Acknowledgments

The authors gratefully acknowledge the financial supports from National Basic Research Program of China (2007CB613303), National High Technology Research and Development Program of China (2006AA06Z377), National Nature Science Foundation of China (50908132) and China Postdoctoral Science Foundation (20090450380).

References

[1] I.M. Arabatzis, T. Stergiopoulos, D. Andreeva, S. Kitova, S.G. Neophytides, P. Falaras, J. Catal. 220 (2003) 127–135.
[2] A. Dawson, P.V. Kamat, J. Phys. Chem. B 105 (2001) 960–966.
[3] Y.M. Wu, J.L. Zhang, L. Xiao, F. Chen, Appl. Catal. B: Environ. 88 (2009) 525–532.
[4] V. Subramanian, E. Wolf, P.V. Kamat, J. Phys. Chem. B 105 (2001) 11439–11446.
[5] N. Chandrasekharan, P.V. Kamat, J. Phys. Chem. B 104 (2000) 10851–10857.
[6] P.V. Kamat, J. Phys. Chem. C 111 (2007) 2834–2860.
[7] H. Tada, T. Kiyonaga, S.I. Naya, Chem. Soc. Rev. 38 (2009) 1849–1858.
[8] T. Kiyonaga, M. Fujii, T. Akita, H. Kobayashi, H. Tada, Phys. Chem. Chem. Phys. 10 (2008) 6553–6561.
[9] B.Z. Tian, J.L. Zhang, T.Z. Tong, F. Chen, Appl. Catal. B: Environ. 79 (2008) 394–401.
[10] J. Li, H.C. Zeng, Chem. Mater. 18 (2006) 4270–4277.
[11] E. Bae, W. Choi, Environ. Sci. Technol. 37 (2003) 147–152.
[12] F.B. Li, X.Z. Li, Appl. Catal. A: Gen. 228 (2002) 15–27.
[13] J.W. Yoon, T. Sasaki, N. Koshizaki, Electrochem. Solid State Lett. 5 (2002) A256–A258.
[14] L. Armelao, D. Barreca, G. Bottaro, A. Gasparotto, E. Tondello, Chem. Mater. 16 (2004) 3331–3338.
[15] L. Armelao, D. Barreca, G. Bottaro, A. Gasparotto, C. Maccato, C. Maragno, E. Tondello, U.L. Stangar, M. Bergant, D. Mahne, Nanotechnology 18 (2007) 375709–375716.
[16] R.S. Sonawane, M.K. Dongare, J. Mol. Catal. A: Chem. 243 (2006) 68–76.
[17] T. Kiyonaga, T. Kawahara, H. Tada, Electrochem. Solid State Lett. 9 (2006) E9–E12.
[18] X.Z. Li, C. He, N. Graham, Y.J. Xiong, Appl. Electrochem. 35 (2005) 741–750.
[19] V. Iliev, D. Tomava, R. Todorovska, D. Oliver, L. Petrov, D. Todorovsky, M. Uzunova-Bujnova, Appl. Catal. A: Gen. 313 (2006) 115–121.
[20] M.D. Pérez, E. Otal, S.A. Bilmes, G.J.A.A. Soler-Illia, E.L. Crepaldi, D. Grosso, C. Sanchez, Langmuir 20 (2004) 6879–6886.
[21] J.C. Yu, X.C. Wang, L. Wu, W.K. Ho, L.Z. Zhang, G.T. Zhou, Adv. Funct. Mater. 14 (2004) 1178–1183.
[22] J.H. He, T. Kunitake, Chem. Mater. 16 (2004) 2656–2661.
[23] J.H. He, I. Ichinose, T. Kunitake, A. Nakao, Langmuir 18 (2002) 10005–10010.
[24] N. Chandrasekharan, P.V. Kamat, Nano Lett. 1 (2001) 67–70.
[25] M.N. Patel, R.D. Williams, R.D. May, H. Uchida, J. Stevenson, K.P. Johnston, Chem. Mater. 20 (2008) 6029–6040.
[26] M. Valden, X. Lai, D.W. Goodman, Science 281 (1998) 1647–1650.
[27] M. Haruta, Catal. Today 36 (1997) 153–166.
[28] V. Subramanian, E.E. Wolf, P.V. Kamat, Langmuir 19 (2003) 469–474.
[29] N.F. Zheng, G.D. Stucky, J. Am. Chem. Soc. 128 (2006) 14278–14280.
[30] M. Comotti, W.C. Li, B. Spliethoff, F. Schth, J. Am. Chem. Soc. 128 (2006) 917–924.
[31] Z.Y. Zhong, J.Y. Lin, S.P. Teh, J. Teo, F.M. Dautzenberg, Adv. Funct. Mater. 17 (2007) 1402–1408.
[32] T.A. Hanaoka, H.P. Kormann, M. Kröll, T. Sawitowski, G. Schmid, Eur. J. Inorg. Chem. 1998 (1998) 807–812.
[33] J. Li, H.C. Zeng, Angew. Chem. Int. Ed. 44 (2005) 4342–4345.
[34] J. Oudar, E.E. Petersen, A.T. Bell, Catalyst Deactivation, Marcel Dekker, New York, 1987.
[35] J.D. Grunwaldt, C. Kiener, C. Wögerbauer, A. Baiker, J. Catal. 181 (1999) 223–232.
[36] I. Gültekin, N.H. Ince, J. Environ. Manage. 85 (2007) 816–832.

[37] Y. Ohko, I. Ando, C. Niwa, T. Tatsuma, T. Yamamura, T. Nakashima, Y. Kubota, A. Fujishima, Environ. Sci. Technol. 35 (2001) 2365–2368.
[38] S. Fukahori, H. Ichiura, T. Kitaoka, H. Tanaka, Appl. Catal. B: Environ. 46 (2003) 453–462.
[39] L. Zhang, P.Y. Zhang, C.S. Chen, Chin. J. Catal. 28 (2007) 299–306.
[40] K.C. Grabar, R.G. Freeman, M.B. Hommer, M.J. Natan, Anal. Chem. 67 (1995) 735–743.
[41] Y.D. Jin, X.F. Kang, Y.H. Song, B.L. Zhang, G.J. Cheng, S.J. Dong, Anal. Chem. 73 (2001) 2843–2849.
[42] H.X. Li, Z.F. Bian, J. Zhu, Y.N. Huo, H. Li, Y.F. Lu, J. Am. Chem. Soc. 129 (2007) 4538–4539.
[43] M. Bowker, D. James, P. Stone, R. Bennett, N. Perkins, L. Millard, J. Greaves, A. Dickinson, J. Catal. 217 (2003) 427–433.
[44] I. Dolamic, C. Gautier, J. Boudon, N. Shalkevich, T. Brgi, J. Phys. Chem. C 112 (2008) 5816–5824.
[45] C.I. Carlens, K.J. Klabunde, Langmuir 16 (2000) 3764–3772.
[46] H. Tsunoyama, H. Sakurai, T. Tsukuda, Chem. Phys. Lett. 429 (2006) 528–532.
[47] H. Tsunoyama, H. Sakurai, N. Ichikuni, Y. Negishi, T. Tsukuba, Langmuir 20 (2004) 11293–11296.
[48] M.M. Alvarez, J.T. Khoury, T.G. Schaaff, M.N. Shafigullin, I. Vezmar, R.L. Whetten, J. Phys. Chem. B 101 (1997) 3706–3712.
[49] Q. Fu, H. Saltsburg, M. Flytzani-Stephanopoulos, Science 301 (2003) 935–938.
[50] C.D. Zangmeister, L.B. Picraux, R.D. Vanzee, Y.X. Yao, J.M. Tour, Chem. Phys. Lett. 442 (2007) 390–393.
[51] T. Ioannides, X.E. Verykios, J. Catal. 161 (1996) 560–569.
[52] C. Mottet, G. Tréglia, B. Legrand, Surf. Sci. 352–354 (1996) 675–679.
[53] P.V. Kamat, M. Flumiani, A. Dawson, Colloids Surf. A 202 (2002) 269–279.
[54] V. Subramanian, E.E. Wolf, P.V. Kamat, J. Am. Chem. Soc. 126 (2004) 4943–4950.
[55] V. Iliev, D. Tomova, L. Bilyarska, G. Tyuliev, J. Mol. Catal. A: Chem. 263 (2007) 32–38.
[56] A. Orlov, D.A. Jefferson, N. Macleod, R.M. Lambert, Catal. Lett. 92 (2004) 41–47.